JACS
JOURNAL OF THE AMERICAN CHEMICAL SOCIETY
pubs.acs.org/JACS
Communication

Boosting Activity and Stability of Metal Single-Atom Catalysts via Regulation of Coordination Number and Local Composition

Leilei Wang,[‡] Chuwei Zhu,[‡] Mingquan Xu, Chuanlin Zhao, Jian Gu, Lina Cao, Xiaohui Zhang, Zhihu Sun, Shiqiang Wei, Wu Zhou, Wei-Xue Li,* and Junling Lu*

Cite This: *J. Am. Chem. Soc.* 2021, 143, 18854−18858
Read Online
ACCESS | Metrics & More | Article Recommendations | Supporting Information

ABSTRACT: Controlling the chemical environments of the active metal atom including both coordination number (CN) and local composition (LC) is vital to achieve active and stable single-atom catalysts (SACs), but remains challenging. Here we synthesized a series of supported Pt_1 SACs by depositing Pt atoms onto the pretuned anchoring sites on nitrogen-doped carbon using atomic layer deposition. In hydrogenation of *para*-chloronitrobenzene, the Pt_1 SAC with a higher CN about four but less pyridinic nitrogen (N_{pyri}) content exhibits a remarkably high activity along with superior recyclability compared to those with lower CNs and more N_{pyri}. Theoretical calculations reveal that the four-coordinated Pt_1 atoms with about 1 eV lower formation energy are more resistant to agglomerations than the three-coordinated ones. Composition-wise decrease of the Pt−N_{pyri} bond upshifts gradually the Pt-5*d* center, and minimal one Pt−N_{pyri} bond features a high-lying Pt-5*d* state that largely facilitates H_2 dissociation, boosting hydrogenation activity remarkably.

Single-atom catalysis, one frontier in heterogeneous catalysis,[1,2] holds promise toward not only a fundamental understanding of catalytic reactions but also practical applications, owing to well-defined structures, maximized atom utilization, and distinct energetics.[3−6] The metal atom (M_1) does not necessarily drive catalytic reactions alone, but often jointly with the coordinated atoms.[7−10] Therefore, the chemical environment of M_1 including both coordination number (CN) and local composition (LC) governs the overall catalytic performance of single-atom catalysts (SACs).[11−13] However, the underlying physics of the CN and LC of SACs on activity, selectivity, and stability is elusive, and how to prepare the SACs with desired CN and LC remains challenging.

Among others, nitrogen-doped carbon (NC) is one impressive support for SACs owing to concentration-controllable N doping for high metal loadings and strong metal−N covalent bonding for high stability. A number of M_1/NC SACs have been successfully synthesized for various catalytic reactions.[5,12,14−17] Nonetheless, achieving an atomic-level understanding of structure−activity relationships is inhibited by the lack of accurate identification of the coordination structure, including both CN and LC, of M_1 even with state-of-the-art characterization techniques, such as X-ray absorption spectroscopy (XAS). Moreover, M_1/NC SACs were often prepared by impregnating/grafting metal precursors into the NC supports followed by high-temperature thermal treatments.[14,15] These synthesis approaches might generate heterogeneous metal atoms with diverse chemical environments, further obscuring the structure characterization. Controlling the CN and LC of M_1 on supports and unveiling the underlying mechanism from first-principles calculations become an urgent need to develop highly active and stable SACs.

Atomic layer deposition (ALD) relies on sequential molecular-level self-limiting surface reactions.[18,19] Control of anchoring sites on the support allows controlling the initial nucleation of metal precursors.[20,21] Here we synthesized a series of Pt_1/NC SACs with different coordination structures in two steps (Figure 1a): (i) Preparation of a series of NC supports with different pyridinic nitrogen (N_{pyri})-related anchoring sites by varying calcination temperature and time; (ii) precise deposition of Pt atoms onto these anchoring sites using Pt ALD. In the hydrogenation of *para*-chloronitrobenzene (*p*-CNB), these Pt_1/NC SACs showed very different catalytic performance. Density functional theory (DFT) calculations unveiled the impact of CNs and LCs on stability and hydrogenation activity and identified Pt_1−N_1C_3 as the active sites for hydrogenations.

The precursor (g-C_3N_4@Glu) of the NC support was first synthesized by hydrothermal treatments of mixtures of g-C_3N_4 and glucose (Figure 1a).[22] Then, a series of NC supports with different N contents were obtained via calcination at 600, 800, 900, and 1000 °C for 1 h, as well as 1000 °C for 3 h under an Ar atmosphere, which are denoted as NC-600, NC-800, NC-900, NC-1000-1h, and NC-1000-3h, respectively. Transmission electron microscopy (TEM) showed that all these NCs had a similar two-dimentional nanosheet-like morphology, containing both micro- and mesoporosities (Figures S1 and S2), and abundant defects according to the observation of

Received: September 8, 2021
Published: November 3, 2021

https://doi.org/10.1021/jacs.1c09498
J. Am. Chem. Soc. 2021, 143, 18854−18858

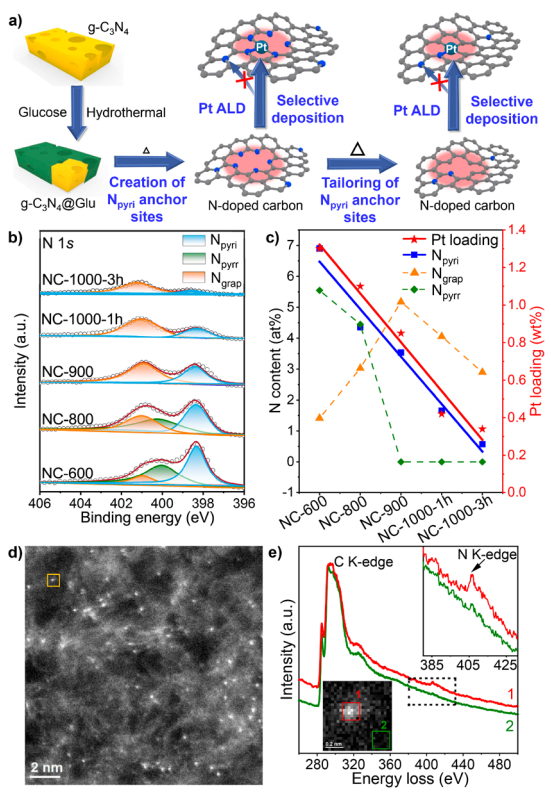

Figure 1. (a) Schematic illustration of the synthesis of Pt_1/NC SACs. (b) XPS spectra of NC supports in the N 1s region. (c) The contents of N_{pyri}, N_{pyrr}, and N_{grap} according to XPS and the Pt loadings in these Pt_1/NC SACs. (d) Representative HAADF-STEM image of Pt_1/NC-1000-3h. (e) Atomic-resolution EELS spectra taken at the locations 1 and 2 of the inset of the STEM image. Therein, the STEM inset image in (e) is an enlargement of the orange rectangle area in (d). Another inset in (e) shows the enlargement of the EELS spectra in the dotted rectangular area.

disordered sp^3 carbon (D band) at 1350 cm^{-1} by Raman spectroscopy (Figure S3).[22] X-ray photoemission spectroscopy (XPS) measurements showed that the N content gradually decreased as the thermal treatment temperature increased (Figure 1b and Table S1).

Pt ALD was carried out on these supports at 150 °C to synthesize Pt_1/NC SACs.[8] The Pt loadings were 1.3, 1.1, 0.85, 0.42, and 0.34 wt % for Pt_1/NC-600, Pt_1/NC-800, Pt_1/NC-900, Pt_1/NC-1000-1h, and Pt_1/NC-1000-3h, respectively (Table S2). While we found that Pt did not nucleate on the pure carbon support (achieved by thermally treating glucose only at 1000 °C for 3 h in Ar), indicating preferential nucleation of Pt at N-related anchoring sites. Correlation of Pt loadings with different N content across all Pt_1/NC SACs revealed that only N_{pyri} exhibited a similar trend with Pt loadings (Figure 1c), indicating the nucleation of Pt mainly at N_{pyri}-related sites. Aberration-corrected high-angle annular dark-field scanning transmission electron microscopy (HAADF-STEM), along with elemental mappings, confirmed the atomic dispersion of Pt in all these samples free from Pt clusters/NPs (Figures S4–S9). State-of-the-art atomic-resolution electron energy-loss spectroscopy (EELS) spectroscopy and mapping further confirmed the existence of a N K-edge signal at the location of the Pt atom (Figure 1d,e and Figure S10).

Fourier-transformed extended X-ray absorption fine structure (EXAFS) spectra showed that all these samples had a peak at ~1.65 Å assigned to Pt–C/N coordination, with considerably increased intensity for the samples from Pt_1/NC-600 to Pt_1/NC-1000-3h (Figure 2a). The CNs are 3.0, 3.2,

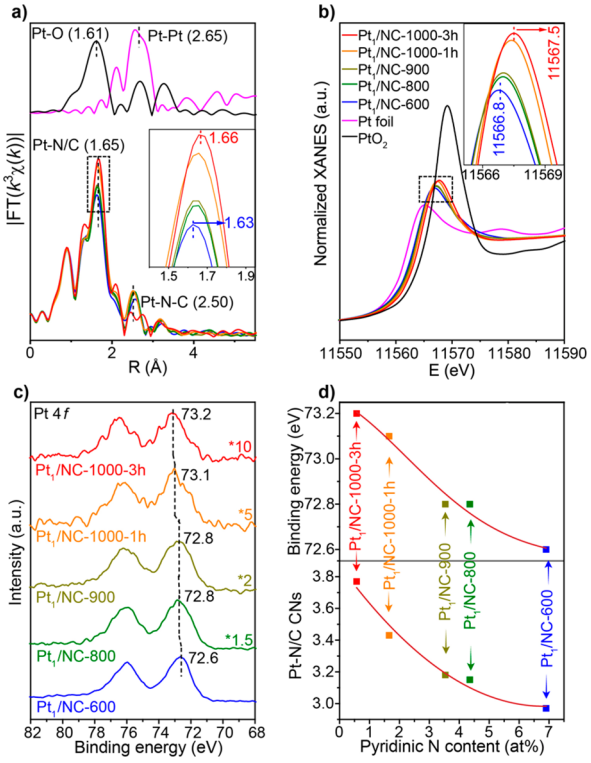

Figure 2. (a) EXAFS and (b) XANES spectra of Pt_1/NC SACs, Pt foil, and PtO_2 reference at the Pt L_3-edge. The insets in (a) and (b) show the corresponding local enlargements of the dashed square areas. The legends in (b) also apply to (a). (c) XPS spectra of Pt_1/NC SACs in the Pt 4f region. (d) The changes of Pt 4f7/2 binding energy and Pt–C/N CNs as a function of N_{pyri} content.

3.2, 3.4, and 3.8, for the samples from Pt_1/NC-600 to Pt_1/NC-1000-3h, respectively, along with a Pt–C/N bond distance of about 2.02–2.05 Å (Figure S11 and Table S3). Wavelet transform plots of Pt_1/NC SACs show that the weak peak at 2.50 Å is ascribed to the secondary shell of the Pt–C/N bond (Figure S12),[17,23] rather than the Pt–Pt coordination (2.65 Å), excluding the presence of Pt clusters/NPs, in-line with the STEM.

X-ray absorption near-edge structure (XANES) spectra showed that the white line peaks of these Pt_1 SACs were between those of Pt foil and PtO_2. The intensities followed the order Pt_1/NC-600 < Pt_1/NC-800 < Pt_1/NC-900 < Pt_1/NC-1000-1h < Pt_1/NC-1000-3h, along with a peak shift from 11 566.8 to 11 567.5 eV (Figure 2b), suggesting that the Pt_1 atoms become more electron deficient as the support was treated at higher temperatures.[24,25] XPS showed a similar trend that the Pt 4f7/2 binding energy shifted considerably from 72.6 eV for Pt_1/NC-600 to higher values, e.g., 73.2 eV for Pt_1/NC-1000-3h (Figure 2c and Figure S13), which were all close to a +2 oxidation state.[26] Figure 2d shows that Pt_1/NC-600 had a higher N_{pyri} content and a lower Pt–C/N CN, whereas Pt_1/NC-1000-3h had a lower N_{pyri} content and a higher Pt–C/N CN with a higher oxidation state.

https://doi.org/10.1021/jacs.1c09498
J. Am. Chem. Soc. 2021, 143, 18854–18858

Haloanilines (HANs) are key intermediates for pharmaceuticals, polymers, agrochemicals, and dyes.[27] Here hydrogenation of *p*-CNB to *para*-chloroaniline (*p*-CAN) was selected as a probe reaction to evaluate their catalytic performance. We found that a considerable amount of *para*-chloronitrosobenzene, a semihydrogenation product, was produced at the initial stage, but was further hydrogenated to *p*-CAN for all Pt_1/NC SACs (Figure S14). There was no dehalogenated aniline (AN) formation even when the reaction was further extended for another 1 or 2 h after the complete conversion. Calculated turnover frequencies (TOFs) based on the Pt content showed that the corresponding activities at 65 °C and a H_2 pressure of 3 bar varied from 360 to 19 600 h^{-1}, where Pt_1/NC-1000-3h had the highest activity, i.e., 54-fold higher than Pt_1/NC-600 (Figure 3a), among the highest values in the literature (Table S4). Kinetic measurements also revealed a lowest apparent activation energy on Pt_1/NC-1000-3h, confirming its extraordinary activity (Figure S15). Similar phenomena were also observed in hydrogenation of nitrobenzene, 3-chloronitrobenzene, and styrene (Figure S16). Besides the above, Pt_1/NC-1000-3h also exhibited excellent recyclability without any obvious Pt leaching/aggregations or structure changes (Figure 3b, Figures S17 and S18, and Table S2). In contrast, all other samples deactivated quickly due to severe Pt leaching and considerable metal aggregation (Figures S19−S22). We note that a Pt/NC NP sample also showed obvious deactivation (Figure S23 and Table S2).

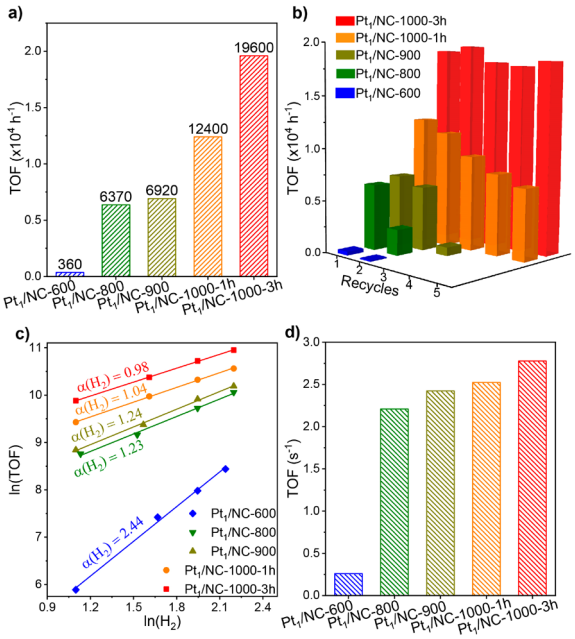

Figure 3. (a) Catalytic activity of Pt_1/NC SACs in hydrogenation of *p*-CNB at 65 °C and a H_2 pressure of 3 bar. (b) Catalyst recycling test on Pt_1/NC SACs. (c) H_2 reaction orders of Pt_1/NC SACs. (d) TOFs of Pt_1/NC SACs in the H−D exchange reaction at 65 °C.

The H_2 reaction order was found as high as 2.44 for Pt_1/NC-600 (Figure 3c), implying H_2 activation is difficult and the rate-limiting step, while the H_2 reaction order decreased considerably on other samples, in line with the trend of hydrogenation activity (Figure 3a). H−D exchange reactions showed a similar trend (Figure 3d), and the corresponding TOF on Pt_1/NC-1000-3h was 2.8 s^{-1}, 11-fold higher than Pt_1/NC-600. Remarkable H_2 activation could be one major reason for its high activity.

For DFT calculations, various $Pt_1-N_xC_y$ structures were constructed, including Pt_1-N_3, $Pt_1-N_2C_1$, and $Pt_1-N_1C_2$ (CN = 3) and Pt_1-N_4, $Pt_1-N_3C_1$, $Pt_1-N_2C_2$, and $Pt_1-N_1C_3$ (CN = 4), where all N are N_{pyri} (Figure S24). The optimized Pt−C and Pt−N_{pyri} bond lengths vary from 1.91 to 2.11 Å (Table S5), in agreement with the measurements. All structures considered are stable for exclusive exothermic formation energies with respect to Pt bulk metal from −1.20 to −2.81 eV (Table S6). Notably, the formation energies for CN = 4 are 1 eV lower than CN = 3. This corroborates excellently with experiments, where the Pt_1/NC SACs with higher CNs had much less extents of sintering and leaching.

Reactivities of $Pt_1-N_xC_y$ toward H_2 dissociation were calculated (Figures S25−S28). H_2 dissociation on Pt_1-N_4 is highly endothermic by 1.86 eV for the homolytic path and 2.40 eV for the heterolytic path, which cannot happen under the mild reaction condition here. With a decrease of the number of Pt_1-N_{pyri} bonds (CN = 4), the reaction energy and kinetic barrier decrease (Table S7) as plotted in Figure 4a for the most favorable paths. For $Pt_1-N_1C_3$ with one Pt_1-N_{pyri} bond, its reaction energy becomes exothermic by −0.26 eV via the heterolytic path over the Pt_1-C pair with a modest barrier of

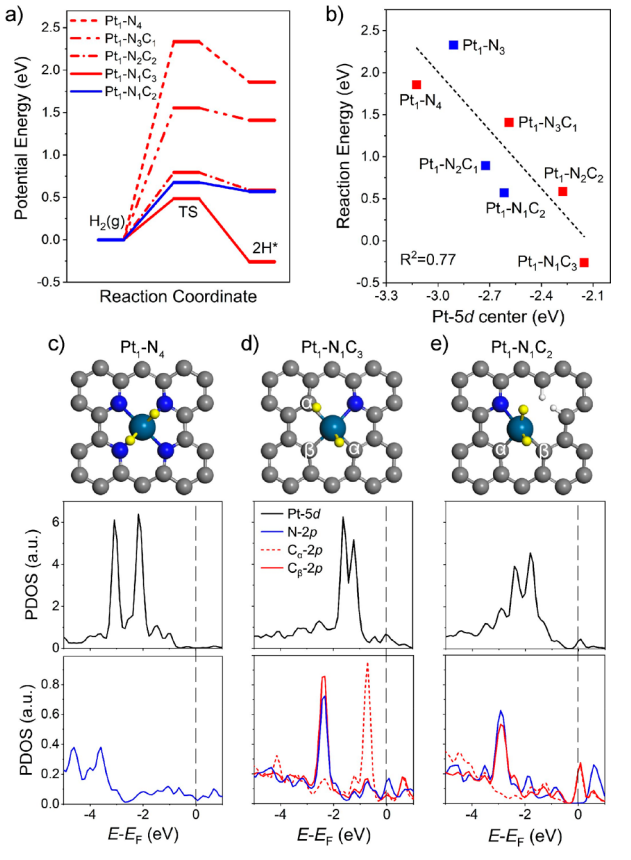

Figure 4. (a) Potential energy profile for H_2 dissociation on Pt_1-N_4, $Pt_1-N_3C_1$, $Pt_1-N_2C_2$, $Pt_1-N_1C_3$, and $Pt_1-N_1C_2$ surfaces. (b) Scaling relationship between the favorable reaction energies of H_2 dissociation and the Pt-5d center. Schematic structures and the corresponding projected density of states of Pt-5d, N-2p, and C-2p orbitals in (c) Pt_1-N_4, (d) $Pt_1-N_1C_3$, and (e) $Pt_1-N_1C_2$, respectively. Gray for carbon, yellow for dissociated H atom, blue for N, and cyan for Pt.

https://doi.org/10.1021/jacs.1c09498
J. Am. Chem. Soc. 2021, 143, 18854−18858

0.48 eV. A similar trend was found for CN = 3 (Table S7), where fewer Pt_1-N_{pyri} bonds is favorable. For $Pt_1-N_1C_2$, the homolytic path was the most favorable with a barrier of 0.68 eV. However, its endothermic energy of 0.57 eV leads to a facile reverse reaction with a barrier of only 0.11 eV. Accordingly, $Pt_1-N_1C_3$ was proposed as the active sites for the most active and stable Pt_1/NC-1000-3h catalyst. CN = 4 and only one Pt_1-N_{pyri} bond are in-line with the experiments of high CN and low N_{pyri} content. For samples with lower CN and more N_{pyri}, $Pt_1-N_1C_3$ is less populated, resulting in a lower reactivity.

To understand the effect of the CN and LC on H_2 dissociation (Figure S29), favorable H_2 dissociation energies on all $Pt_1-N_xC_y$ structures considered against the Pt-5*d* center ϵ_{5d} are shown in Figure 4c–e and Figure S30. It was found that the higher the ϵ_{5d} is, the more favorable the reaction energy. Upshift of ϵ_{5d} comes along with a decrease of the $Pt-N_{pyri}$ bond, due to the weakened $Pt-N_{pyri}$ hybridization. Compared to 3CN $Pt_1-N_1C_2$ (Figure 4e), the extent of the Pt–N hybridization in 4CN $Pt_1-N_1C_3$ is further weakened (Figure 4d), resulting in an even higher ϵ_{5d}. Moreover, the neighbor carbon atom C_α in $Pt_1-N_1C_3$ has a considerable number of states right below the Fermi level, but are absent in $Pt_1-N_1C_2$. These electronic properties activate the corresponding C_α and result in a facile dissociation over the Pt_1-C_α (Figures 4b, S31, and S32, Table S8), in contrast to $Pt_1-N_1C_2$.

In summary, we have synthesized a series of Pt_1/NC SACs by precisely depositing Pt atoms onto N_{pyri} anchoring sites using ALD. We demonstrated that Pt_1/NC SACs with high CN and less N_{pyri} prepared via extended high calcination temperature exhibited higher hydrogenation activity of *p*-CNB and excellent recyclability. DFT calculations disclosed that the 4CN Pt_1 atoms have more resistant to agglomeration and leaching than the 3CN ones and a decrease in the Pt_1-N_{pyri} bond upshift in the corresponding Pt-5*d* center. $Pt_1-N_1C_3$ was proposed as the active sites for hydrogenations. Such decisive roles of CNs and LCs on the catalytic performance of SACs provide critical insight into the rational design of SACs with high activity and stability.

■ ASSOCIATED CONTENT

Supporting Information

The Supporting Information is available free of charge at https://pubs.acs.org/doi/10.1021/jacs.1c09498.

Experimental details, additional characterization data, and catalytic performance tests as well as optimized structures deposited at Zenodo[28] (PDF)

■ AUTHOR INFORMATION

Corresponding Authors

Junling Lu − *Hefei National Laboratory for Physical Sciences at the Microscale, Department of Chemical Physics, School of Chemistry and Materials Science, University of Science and Technology of China, Hefei, Anhui 230026, China;* orcid.org/0000-0002-2607-6869; Email: junling@ustc.edu.cn

Wei-Xue Li − *Hefei National Laboratory for Physical Sciences at the Microscale, Department of Chemical Physics, School of Chemistry and Materials Science, University of Science and Technology of China, Hefei, Anhui 230026, China;* orcid.org/0000-0002-5043-3088; Email: wxli70@ustc.edu.cn

Authors

Leilei Wang − *Hefei National Laboratory for Physical Sciences at the Microscale, Department of Chemical Physics, School of Chemistry and Materials Science, University of Science and Technology of China, Hefei, Anhui 230026, China;* orcid.org/0000-0003-1039-0762

Chuwei Zhu − *Hefei National Laboratory for Physical Sciences at the Microscale, Department of Chemical Physics, School of Chemistry and Materials Science, University of Science and Technology of China, Hefei, Anhui 230026, China*

Mingquan Xu − *School of Physical Sciences, CAS Key Laboratory of Vacuum Physics, CAS Center for Excellence in Topological Quantum Computation, University of Chinese Academy of Sciences, Beijing 100049, China;* orcid.org/0000-0002-2033-437X

Chuanlin Zhao − *Hefei National Laboratory for Physical Sciences at the Microscale, Department of Chemical Physics, School of Chemistry and Materials Science, University of Science and Technology of China, Hefei, Anhui 230026, China*

Jian Gu − *Hefei National Laboratory for Physical Sciences at the Microscale, Department of Chemical Physics, School of Chemistry and Materials Science, University of Science and Technology of China, Hefei, Anhui 230026, China*

Lina Cao − *Hefei National Laboratory for Physical Sciences at the Microscale, Department of Chemical Physics, School of Chemistry and Materials Science, University of Science and Technology of China, Hefei, Anhui 230026, China*

Xiaohui Zhang − *Hefei National Laboratory for Physical Sciences at the Microscale, Department of Chemical Physics, School of Chemistry and Materials Science, University of Science and Technology of China, Hefei, Anhui 230026, China*

Zhihu Sun − *National Synchrotron Radiation Laboratory, University of Science and Technology of China, Hefei, Anhui 230029, China;* orcid.org/0000-0002-3898-969X

Shiqiang Wei − *National Synchrotron Radiation Laboratory, University of Science and Technology of China, Hefei, Anhui 230029, China;* orcid.org/0000-0002-2052-1132

Wu Zhou − *School of Physical Sciences, CAS Key Laboratory of Vacuum Physics, CAS Center for Excellence in Topological Quantum Computation, University of Chinese Academy of Sciences, Beijing 100049, China*

Complete contact information is available at: https://pubs.acs.org/10.1021/jacs.1c09498

Author Contributions

‡W.L. and Z.C. contributed equally to this work.

Notes

The authors declare no competing financial interest.

■ ACKNOWLEDGMENTS

This work was supported by the National Natural Science Foundation of China (22025205, 91945302), DNL Cooperation Fund, CAS (DNL201907, DNL201920), the Fundamental Research Funds for the Central Universities (WK2060030029), the National Key R&D Program of China (2018YFA0208603), Chinese Academy of Sciences (QYZDJ-SSW-SLH054), K. C. Wong Education (GJTD-2020-15), and Users with Excellence Program of Hefei Science Center CAS (2019HSCUE016) and used high-performance

computational resources provided by University of Science and Technology of China and National Supercomputing Center in Zhengzhou. The authors also gratefully thank the staff at the BL14W1 beamline at the Shanghai Synchrotron Radiation Facility (SSRF) and the BL10B beamlines at National Synchrotron Radiation Laboratory (NSRL), China.

REFERENCES

(1) Pelletier, J. D.; Basset, J. M. Catalysis by Design: Well-Defined Single-Site Heterogeneous Catalysts. *Acc. Chem. Res.* **2016**, *49* (4), 664−677.
(2) Wang, A.; Li, J.; Zhang, T. Heterogeneous single-atom catalysis. *Nat. Rev. Chem.* **2018**, *2* (6), 65−81.
(3) Deng, D.; Chen, X.; Yu, L.; Wu, X.; Liu, Q.; Liu, Y.; Yang, H.; Tian, H.; Hu, Y.; Du, P.; Si, R.; Wang, J.; Cui, X.; Li, H.; Xiao, J.; Xu, T.; Deng, J.; Yang, F.; Duchesne, P. N.; Zhang, P.; Zhou, J.; Sun, L.; Li, J.; Pan, X.; Bao, X. A single iron site confined in a graphene matrix for the catalytic oxidation of benzene at room temperature. *Sci. Adv.* **2015**, *1* (11), e1500462.
(4) Liu, G.; Robertson, A. W.; Li, M. M.; Kuo, W. C. H.; Darby, M. T.; Muhieddine, M. H.; Lin, Y. C.; Suenaga, K.; Stamatakis, M.; Warner, J. H.; Tsang, S. C. E. MoS_2 monolayer catalyst doped with isolated Co atoms for the hydrodeoxygenation reaction. *Nat. Chem.* **2017**, *9* (8), 810−816.
(5) Zhang, Z.; Chen, Y.; Zhou, L.; Chen, C.; Han, Z.; Zhang, B.; Wu, Q.; Yang, L.; Du, L.; Bu, Y.; Wang, P.; Wang, X.; Yang, H.; Hu, Z. The simplest construction of single-site catalysts by the synergism of micropore trapping and nitrogen anchoring. *Nat. Commun.* **2019**, *10* (1), 1657.
(6) Sarma, B. B.; Plessow, P. N.; Agostini, G.; Concepcion, P.; Pfander, N.; Kang, L.; Wang, F. R.; Studt, F.; Prieto, G. Metal-Specific Reactivity in Single-Atom Catalysts: CO Oxidation on 4d and 5d Transition Metals Atomically Dispersed on MgO. *J. Am. Chem. Soc.* **2020**, *142* (35), 14890−14902.
(7) Qiao, B.; Wang, A.; Yang, X.; Allard, L. F.; Jiang, Z.; Cui, Y.; Liu, J.; Li, J.; Zhang, T. Single-atom catalysis of CO oxidation using Pt_1/FeO_x. *Nat. Chem.* **2011**, *3* (8), 634−641.
(8) Wang, C.; Gu, X.-K.; Yan, H.; Lin, Y.; Li, J.; Liu, D.; Li, W.-X.; Lu, J. Water-Mediated Mars−Van Krevelen Mechanism for CO Oxidation on Ceria-Supported Single-Atom Pt_1 Catalyst. *ACS Catal.* **2017**, *7* (1), 887−891.
(9) Vile, G.; Albani, D.; Nachtegaal, M.; Chen, Z.; Dontsova, D.; Antonietti, M.; Lopez, N.; Perez-Ramirez, J. A stable single-site palladium catalyst for hydrogenations. *Angew. Chem., Int. Ed.* **2015**, *54* (38), 11265−11269.
(10) Gu, X.-K.; Qiao, B.; Huang, C.-Q.; Ding, W.-C.; Sun, K.; Zhan, E.; Zhang, T.; Liu, J.; Li, W.-X. Supported Single Pt_1/Au_1 Atoms for Methanol Steam Reforming. *ACS Catal.* **2014**, *4* (11), 3886−3890.
(11) Liu, P.; Zhao, Y.; Qin, R.; Mo, S.; Chen, G.; Gu, L.; Chevrier, D. M.; Zhang, P.; Guo, Q.; Zang, D.; Wu, B.; Fu, G.; Zheng, N. Photochemical route for synthesizing atomically dispersed palladium catalysts. *Science* **2016**, *352* (6287), 797−801.
(12) Wang, Z.-L.; Choi, J.; Xu, M.; Hao, X.; Zhang, H.; Jiang, Z.; Zuo, M.; Kim, J.; Zhou, W.; Meng, X.; Yu, Q.; Sun, Z.; Wei, S.; Ye, J.; Wallace, G. G.; Officer, D. L.; Yamauchi, Y. Optimizing Electron Densities of Ni-N-C Complexes by Hybrid Coordination for Efficient Electrocatalytic CO_2 Reduction. *ChemSusChem* **2020**, *13* (5), 929−937.
(13) Li, J.; Guan, Q.; Wu, H.; Liu, W.; Lin, Y.; Sun, Z.; Ye, X.; Zheng, X.; Pan, H.; Zhu, J.; Chen, S.; Zhang, W.; Wei, S.; Lu, J. Highly Active and Stable Metal Single-Atom Catalysts Achieved by Strong Electronic Metal−Support Interactions. *J. Am. Chem. Soc.* **2019**, *141* (37), 14515−14519.
(14) Zhou, Y.; Tao, X.; Chen, G.; Lu, R.; Wang, D.; Chen, M.; Jin, E.; Yang, J.; Liang, H.; Zhao, Y.; Feng, X.; Narita, A.; Mullen, K. Multilayer stabilization for fabricating high-loading single-atom catalysts. *Nat. Commun.* **2020**, *11* (1), 5892.
(15) Qu, Y.; Li, Z.; Chen, W.; Lin, Y.; Yuan, T.; Yang, Z.; Zhao, C.; Wang, J.; Zhao, C.; Wang, X.; Zhou, F.; Zhuang, Z.; Wu, Y.; Li, Y. Direct transformation of bulk copper into copper single sites via emitting and trapping of atoms. *Nat. Catal.* **2018**, *1* (10), 781−786.
(16) Lin, R.; Albani, D.; Fako, E.; Kaiser, S. K.; Safonova, O. V.; Lopez, N.; Perez-Ramirez, J. Design of Single Gold Atoms on Nitrogen-Doped Carbon for Molecular Recognition in Alkyne Semi-Hydrogenation. *Angew. Chem., Int. Ed.* **2019**, *58* (2), 504−509.
(17) He, X.; He, Q.; Deng, Y.; Peng, M.; Chen, H.; Zhang, Y.; Yao, S.; Zhang, M.; Xiao, D.; Ma, D.; Ge, B.; Ji, H. A versatile route to fabricate single atom catalysts with high chemoselectivity and regioselectivity in hydrogenation. *Nat. Commun.* **2019**, *10* (1), 3663.
(18) Lu, J.; Elam, J. W.; Stair, P. C. Atomic layer deposition—Sequential self-limiting surface reactions for advanced catalyst "bottom-up" synthesis. *Surf. Sci. Rep.* **2016**, *71* (2), 410−472.
(19) George, S. M. Atomic Layer Deposition: An Overview. *Chem. Rev.* **2010**, *110* (1), 111−131.
(20) Yan, H.; Cheng, H.; Yi, H.; Lin, Y.; Yao, T.; Wang, C.; Li, J.; Wei, S.; Lu, J. Single-Atom Pd_1/Graphene Catalyst Achieved by Atomic Layer Deposition: Remarkable Performance in Selective Hydrogenation of 1,3-Butadiene. *J. Am. Chem. Soc.* **2015**, *137* (33), 10484−10487.
(21) Zhang, L.; Si, R.; Liu, H.; Chen, N.; Wang, Q.; Adair, K.; Wang, Z.; Chen, J.; Song, Z.; Li, J.; Banis, M. N.; Li, R.; Sham, T.-K.; Gu, M.; Liu, L.-M.; Botton, G. A.; Sun, X. Atomic layer deposited Pt-Ru dual-metal dimers and identifying their active sites for hydrogen evolution reaction. *Nat. Commun.* **2019**, *10* (1), 4936.
(22) Yu, H.; Shang, L.; Bian, T.; Shi, R.; Waterhouse, G. I.; Zhao, Y.; Zhou, C.; Wu, L. Z.; Tung, C. H.; Zhang, T. Nitrogen-Doped Porous Carbon Nanosheets Templated from g-C_3N_4 as Metal-Free Electrocatalysts for Efficient Oxygen Reduction Reaction. *Adv. Mater.* **2016**, *28* (25), 5080−5086.
(23) Liu, J.; Jiao, M.; Lu, L.; Barkholtz, H. M.; Li, Y.; Wang, Y.; Jiang, L.; Wu, Z.; Liu, D.; Zhuang, L.; Ma, C.; Zeng, J.; Zhang, B.; Su, D.; Song, P.; Xing, W.; Xu, W.; Wang, Y.; Jiang, Z.; Sun, G. High performance platinum single atom electrocatalyst for oxygen reduction reaction. *Nat. Commun.* **2017**, *8* (1), 15938.
(24) Gallezot, P.; Weber, R.; Dallabetta, R. A.; Boudart, M. Investigation by X-Ray Absorption Spectroscopy of Platinum Clusters Supported on Zeolites. *Z. Naturforsch., A: Phys. Sci.* **1979**, *34* (1), 40−42.
(25) Lytle, F. W. Determination of D-Band Occupancy in Pure Metals and Supported Catalysts by Measurement of L_3 X-Ray Absorption Threshold. *J. Catal.* **1976**, *43* (1−3), 376−379.
(26) Pereira-Hernandez, X. I.; DeLaRiva, A.; Muravev, V.; Kunwar, D.; Xiong, H.; Sudduth, B.; Engelhard, M.; Kovarik, L.; Hensen, E. J. M.; Wang, Y.; Datye, A. K. Tuning Pt-CeO_2 interactions by high-temperature vapor-phase synthesis for improved reducibility of lattice oxygen. *Nat. Commun.* **2019**, *10* (1), 1358.
(27) Jones, C. R.; Liu, Y. Y.; Sepai, O.; Yan, H.; Sabbioni, G. Internal exposure, health effects, and cancer risk of humans exposed to chloronitrobenzene. *Environ. Sci. Technol.* **2006**, *40* (1), 387−394.
(28) Wang, L.; Zhu, C.; Xu, M.; Zhao, C.; Gu, J.; Cao, L.; Zhang, X.; Sun, Z.; Wei, S.; Zhou, W.; Li, W.-X.; Lu, J.Boosting Activity and Stability of Metal Single-Atom Catalysts via Regulation of Coordination Number and Local Composition. *Zenodo*, 2021.

https://doi.org/10.1021/jacs.1c09498
J. Am. Chem. Soc. 2021, 143, 18854−18858